Communication

Wideband Back Cover Microstrip Antenna With Multiple Shorting Vias for Mobile 5G MIMO Applications

Mingzhe Hu and Yue Li

***Abstract*— This communication proposes a wideband and low-profile microstrip antenna for multiple-input multiple-output (MIMO) applications. By loading two sets of shorting vias and cutting two symmetrical slots on a rectangular patch, triple modes, including the monopole mode, the TM_{10}, and TM_{01} modes, are excited simultaneously to achieve the wideband radiation in a relatively low profile. Four elements of the proposed antenna are placed in a sequentially rotated configuration for mobile MIMO applications with a small volume of 59.2 × 59.2 × 2.5 mm^3 (0.82 λ_0 × 0.82 λ_0 × 0.034 λ_0, where λ_0 is the free-space wavelength at the center frequency). A cross-line fence is placed in the center to improve the isolation between adjacent elements. A prototype of the proposed MIMO antenna is fabricated and tested, with the measured −6-dB impedance bandwidth of 3.3–5.0 GHz, covering the N77/N78/N79 bands of fifth-generation (5G) requirements. The proposed four-elements MIMO antenna has the advantages of low profile, compact size, and wide bandwidth, providing a feasible solution of 5G mobile MIMO antennas on the back cover of the device.**

***Index Terms*— Fifth generation (5G), microstrip antennas, multiple-input multiple-output (MIMO), sequentially rotated array, wideband antennas.**

I. Introduction

With the development and widespread application of fifth generation (5G), the number of antennas in a typical mobile phone increases obviously and so does the challenge for antenna design. Multiple-input multiple-output (MIMO) is an important technology in mobile 5G applications, and a typical 5G mobile phone consists of at least four antennas. Traditional mobile phones mostly employ antennas at the bezel zone, which has a clearance of several millimeters for MIMO antennas [1], [2], [3], [4], [5], [6], [7]. However, with the increased antenna number and the configuration of full-screen display, the bezel zone is crowded for MIMO antennas. Therefore, antennas on the back cover are an alternative for antenna engineers [8], [9], [10], [11], [12], [13], [14], [15]. In [9], four shorted patches function as the radiator of an antenna pair to cover the N79 band. Half-mode patch [10], [11], planar inverted-F antenna [12], [13], and slot antenna [14] are also utilized to realize multiple narrow bands or wideband radiation. Apart from traditional modes and their varieties, characteristic mode analysis is applied in [15] to design a back cover MIMO antenna with high isolation.

To be integrated with the back cover of the mobile phone, the antenna needs a low profile with a complete ground plane to avoid breaking the mainboard. Among all the antennas, the microstrip antennas are suitable candidates. However, traditional microstrip antennas suffer from narrow bandwidth due to the low profile and high quality factor. Recently, a lot of methods for bandwidth enhancement of microstrip antennas have been reported. The first type uses single-mode perturbation. Two E-shaped patches are proposed to achieve a bandwidth of 9% [16] and 24% [17] with different profiles. The structure is simple, though the design freedom is limited. The second type is widely known as the multiple modes coupling theory [18], [19], [20], [21]. Parasitic stubs, slots, or vias are used to tune multiple modes closer to obtain a wider bandwidth. In [18], shorting vias are employed to couple TM_{10} and TM_{12} modes. With a central slot to provide an additional slot mode, the antenna realizes a bandwidth of 55%. A set of concentric conductive vias are loaded on a circular patch to excite the TM_{01} and TM_{02} modes with a conical radiation pattern in [20] and [21]. However, simultaneously exciting multiple modes at designated frequencies may result in intricate structures and difficulty of independent tuning. The third type is inspired by recent advances in metamaterials [22], [23], [24], [25], [26]. By periodically arranging a square mushroom array in [22] or loading gridded slots on a rectangular patch in [23], [24], and [25], the TM_{10} and antiphase TM_{20} modes are excited and coupled to achieve a rather wide bandwidth of up to 41% with a low profile of less than 0.06 λ_0 (λ_0 is the free-space wavelength at the center frequency). Besides, the concept of composite right-/left-handed transmission line is used in [26] to excite a negative-order resonance. Despite the excellent performance, the metamaterial-inspired antennas suffer from a large footprint and complicated structure.

In this communication, a wideband back cover microstrip antenna is proposed for mobile 5G MIMO applications. Starting from a rectangular microstrip antenna, by loading two sets of shorting vias and cutting two symmetrical slots, the monopole mode, the TM_{10}, and TM_{01} modes are simultaneously excited to cover the N77/N78/N79 bands of 3.3–5.0 GHz. The design process with parametric studies is provided to explicate the working mechanism. Four elements are arranged in a sequentially rotated configuration with a small volume of 59.2 × 59.2 × 2.5 mm^3 (0.82 λ_0 × 0.82 λ_0 × 0.034 λ_0). A cross-line fence is used to improve the isolation between adjacent elements. A prototype of the MIMO antenna is fabricated and tested. The measured results are in agreement with the simulations. Integration with a full cover and user's hand is also studied to validate the compatibility with mobile phones, exhibiting its potential applications for mobile 5G terminals.

II. Antenna Configuration and Working Mechanism

A. Antenna Configuration

The structural configuration of the proposed four-elements MIMO antenna is illustrated in Fig. 1, which shows the exploded, top, and side views. The proposed MIMO antenna consists of two layers: an FR-4 substrate with height h_1 and an air layer with height

Manuscript received 18 April 2023; revised 30 May 2023; accepted 26 June 2023. Date of publication 11 July 2023; date of current version 6 October 2023. This work was supported in part by the National Natural Science Foundation of China under Grant U22B2016 and Grant 62022045, in part by the National Key Research and Development Program of China under Grant 2021YFA0716601, and in part by the Shenzhen Science and Technology Program under Grant JSGG20210802153800002. *(Corresponding author: Yue Li.)*

The authors are with the Department of Electronic Engineering, Beijing National Research Center for Information Science and Technology, Tsinghua University, Beijing 100084, China (e-mail: lyee@tsinghua.edu.cn).

Color versions of one or more figures in this communication are available at https://doi.org/10.1109/TAP.2023.3291802.

Digital Object Identifier 10.1109/TAP.2023.3291802

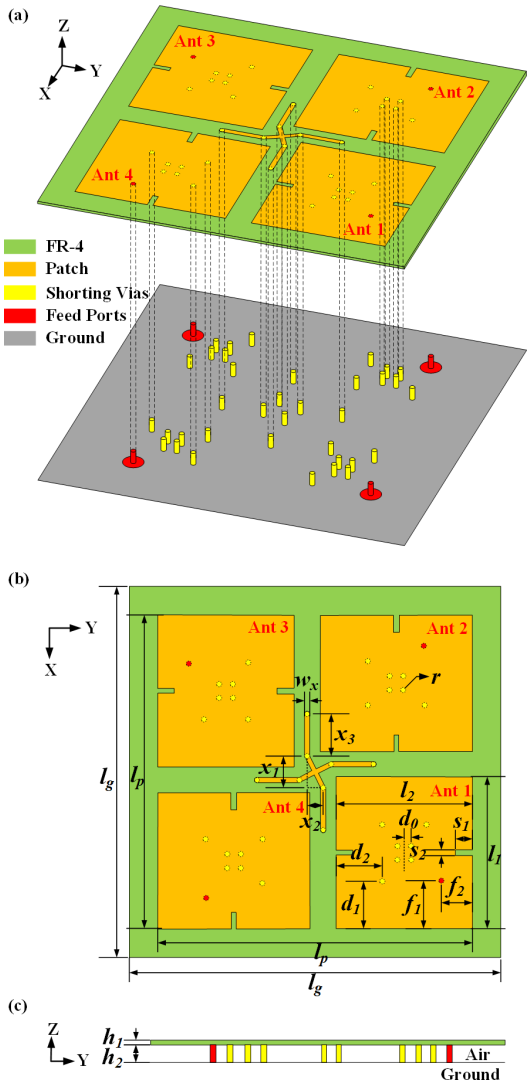

Fig. 1. Configuration of the proposed four-elements MIMO antenna. (a) Exploded view. (b) Top view. (c) Side view.

h_2. A ground plane is at the bottom. The FR-4 substrate has a relative permittivity of 4.4 and a loss tangent of 0.02. The air layer corresponds to the space between the back cover and the mainboard, imitating the typical configuration of mobile phones.

As shown in Fig. 1(b), both the substrate and the ground are in a square shape of $l_g \times l_g$. On the top surface of the substrate are the four same antenna elements arranged in a sequentially rotated configuration, forming an envelope of $l_p \times l_p$. Each antenna consists of a rectangular patch with two symmetric slots etched on the long side and loaded with multiple shorting vias. The dimension of the rectangular patch is $l_1 \times l_2$, and the slots all have a length of s_1 and a width of s_2. For each element, the shorting vias can be divided into two sets. Set 1 consists of three outer vias with their distances to the wide side d_1 and the long side d_2. Set 2 consists of four inner vias at the center of the patch, forming a square of $2d_0$. All the vias with a radius of r connect the patch and the ground plane. Fig. 1(c) only shows part of the shorting vias for simplicity. The feed point is approximately symmetric with the first set of vias but has distances f_1 and f_2 instead. Apart from the four elements, a slightly bent cross-line fence is located in the center. Its shape can be thought of as a cross with its four branches slightly bent clockwise. The dimensions of the fence are marked in Fig. 1(b). The detailed values of each parameter are listed in Table I. The commercial software

TABLE I
DETAILED DIMENSIONS (UNIT: MILLIMETERS)

Parameter	Value	Parameter	Value	Parameter	Value
h_1	0.5	l_g	70.0	d_1	9.0
h_2	2.0	l_p	59.2	d_2	8.7
x_1	6.0	l_1	28.7	d_0	1.3
x_2	3.0	l_2	25.7	f_1	9.15
x_3	8.0	s_1	3.2	f_2	5.85
w_x	1.0	s_2	1.0	r	0.5

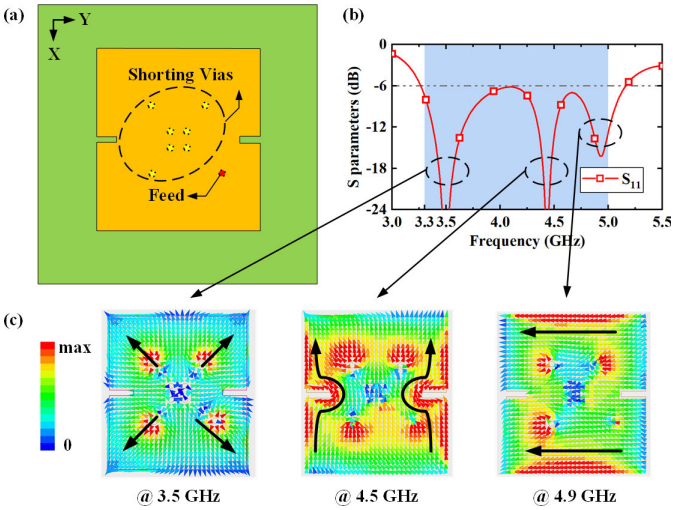

Fig. 2. Antenna element and its working mechanism. (a) Antenna element configuration (top view). (b) Simulated reflection coefficient of the proposed antenna element. (c) Surface current distributions on the patch at three resonant frequencies.

Ansoft high-frequency structure simulator (HFSS) is used for antenna design and optimization.

B. Working Mechanism

Fig. 2 illustrates the details of the proposed antenna element and its working mechanism. Fig. 2(a) shows the top view of a single antenna element, comprising a rectangular patch with two slots, seven shorting vias, and one feed point. The detailed optimized values of its geometry parameters are slightly different from the ones in Table I. For the antenna element, $d_1 = 8.85$ mm, $d_2 = 8.35$ mm, $s_1 = 4.0$ mm, and the others remain the same. The simulated reflection coefficient is given in Fig. 2(b). It shows that the antenna has three resonance frequencies at 3.5, 4.5, and 4.9 GHz, providing a -6-dB impedance bandwidth from 3.26 to 5.16 GHz. Fig. 2(c) plots the surface current distributions on the patch at the three resonant frequencies. At 3.5 GHz, it is observed that currents flow outward from the three outer vias and the feed point. The two currents on the same diagonal are opposite, thus resulting in a radiation null at the broadside, which means a monopole mode is obtained. For 4.5 and 4.9 GHz, currents mostly flow along the long or wide side of the patch, showing a typical TM_{10} or TM_{01} mode. According to the microstrip cavity theory, at the working frequency of TM_{10} mode, the length of the long side approximately equals half of the wavelength, whereas TM_{01} mode corresponds to the wide side. For a rectangular patch, the frequency of TM_{10} mode is naturally lower than that of TM_{01} mode. By etching two symmetric slots on the long sides, the current path is extended, as shown in Fig. 2(c), further lowering the frequency of TM_{10} mode.

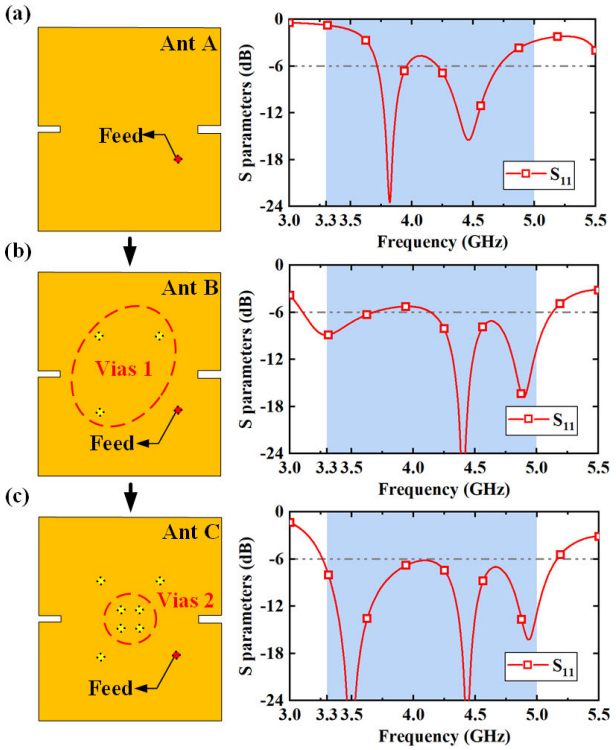

Fig. 3. Design process of the proposed antenna element: structures and reflection coefficients. (a) Ant A: traditional rectangular patch with two symmetric slots etched on the long side. (b) Ant B: add shorting vias 1. (c) Ant C: add shorting vias 2.

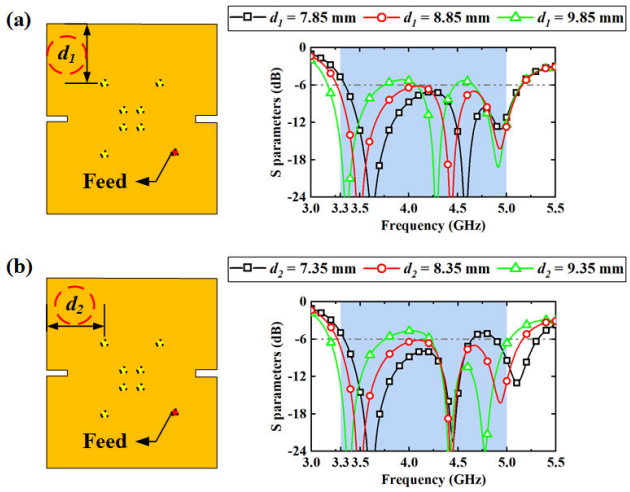

Fig. 4. Reflection coefficients for the proposed antenna element with different values of (a) d_1 and (b) d_2.

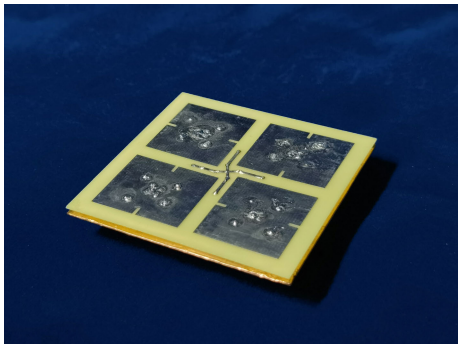

Fig. 5. Photograph of the fabricated four-elements MIMO antenna prototype.

To explain the working mechanism of the antenna, a design process concerning the two sets of shorting vias is shown in Fig. 3. Ant A consists of a rectangular patch with two slots and its dual-band mechanism has been explained above. The simulated result shows its two resonant frequencies at 3.8 and 4.5 GHz. By loading the first set of shorting vias, the monopole mode of Ant B is excited at about 3.3 GHz. Meanwhile, the TM_{10} and TM_{01} modes are shifted higher, which can be explained by the equivalent circuit model. The patch can be seen as a parallel *RLC* resonant circuit. The multiple shorting vias are modeled as parallel inductance, reducing the total equivalent inductance in the circuit. Thus, the resonant frequencies are shifted higher.

Next, we add the second set of shorting vias to get Ant C. Since the vias are at the center where the E-field is close to zero for the TM_{10} and TM_{01} modes, their resonant frequencies are unaffected. Actually, we can see from Fig. 3(c) that these four vias mainly improve the impedance matching of the monopole mode and slightly shift the resonant frequency from 3.3 to 3.5 GHz, closer to the other two modes. The number of the second set of vias is chosen on the compromise of impedance matching and structure simplicity. Therefore, by exciting the monopole mode, the TM_{10} mode, and the TM_{01} mode, we obtain a wideband microstrip antenna covering the frequency band from 3.3 to 5.0 GHz.

To further show how to tune the three modes, some critical parameters of the shoring vias are further studied. Fig. 4 lists two groups of parametric studies with the simulated reflection coefficients. The distances to the two sides are studied carefully for the first set of shorting vias. From Fig. 4(a), the distance d_1 mainly influences the monopole mode and TM_{10} mode. When d_1 gets smaller, the shorting vias are closer to the side. According to the E-field distribution of TM_{10} mode, its strength gets stronger, and hence, the influence of the shorting vias, i.e., shifting the resonant frequencies of the two modes higher, gets more obvious. The same reason applies to d_2, too. Combining d_1 and d_2 together, we can tune the three modes and achieve wideband radiation characteristics.

III. Fabrication and Measurement

A prototype of the proposed four-elements MIMO antenna has been fabricated and tested to validate our design. Fig. 5 shows the photograph of the fabricated prototype. The FR-4 substrate board floats above the copper board (ground plane), held by the multiple shorting vias soldered with the patch and the ground plane. For the feed points, the ground plane is etched with four holes and soldered with four subminiature A (SMA) cable connectors. The outer conductor is connected to the ground plane. The inner conductor extends through the air layer and the FR-4 layer and is soldered with the metallic patch. The S-parameters are measured with a vector network analyzer (Agilent N9917A), and the radiation properties are measured in an anechoic chamber. The simulated and measured results of S-parameters are shown in Fig. 6. For simulation, the reflection coefficients are below −6 dB from 3.24 to 5.00 GHz, covering the N77/N78/N79 band of 3.3–5.0 GHz. Adjacent elements have an isolation of over 11 dB within the operating band, and over 14 dB is achieved between the diagonal ones. For measurement, the −6-dB impedance bandwidth of all four elements is from 3.19 to 4.95 GHz, which covers the three 5G bands. The isolations between two elements are over 12 dB. Fig. 7 plots the total efficiency and the envelope correlation coefficients (ECCs). The simulated total efficiency is over 57% (−2.44 dB) across the band and has a peak of 86% (−0.66 dB). Due to structural symmetry, only the total efficiency

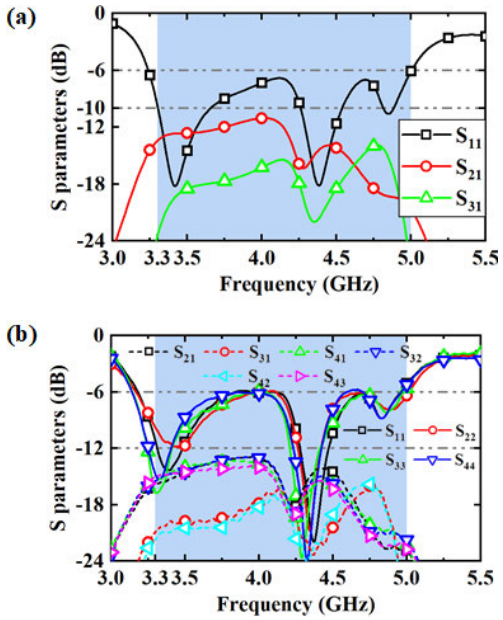

Fig. 6. S-parameters of the four-elements MIMO antenna. (a) Simulated results. (b) Measured results.

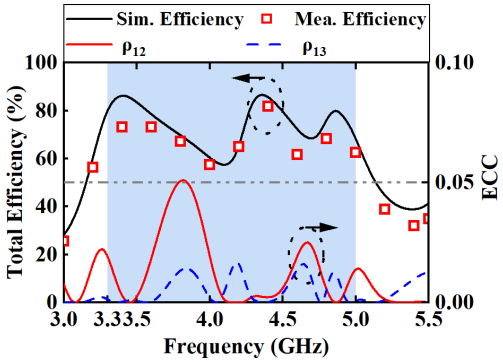

Fig. 7. Total efficiency and the ECCs of the four-elements MIMO antenna.

of Ant 1 is measured, which is from 55% (−2.60 dB) to 82% (−0.86 dB). The ECCs are less than 0.05, which is considerably small for mobile MIMO antennas.

Fig. 8 shows the radiation patterns of the proposed MIMO antenna at three typical working frequencies. At 3.4 GHz, the antenna element works in the monopole mode, but the pattern at 3.4 GHz of the proposed MIMO antenna does not show an obvious radiation null, mainly due to the out-of-center position on the whole substrate and the interaction with the cross-line fence, which is advantageous in mobile communication. The patterns at 4.4 and 4.9 GHz show a broadside property and correspond well to the TM_{10} and TM_{01} modes. The realized gains at three frequencies are 5.19, 8.82, and 8.08 dBi and range from 4.43 to 8.87 dBi across the band. The measurement results are basically in accord with the simulations.

IV. Discussion

For the proposed MIMO antenna, a cross-line fence is added among the four antenna elements. Many decoupling methods have been proposed in previous works. For example, shorting vias or metal walls are used in [27] and [28] to create a physical blockage for decoupling. Besides, slots or metal rings are placed between antennas to create a new resonant current, which cancels out the original coupling [29], [30]. Recently, orthogonal modes [31] and the method

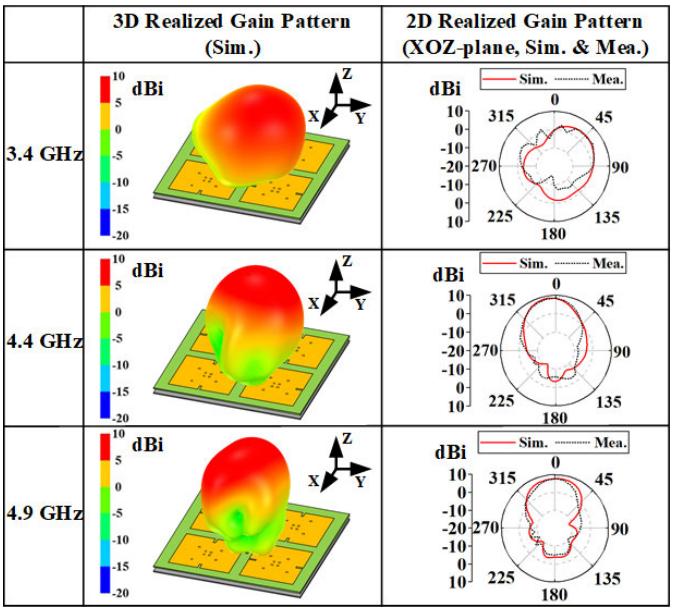

Fig. 8. Three-dimensional and 2-D radiation patterns of the four-elements MIMO antenna (only Ant 1 is excited).

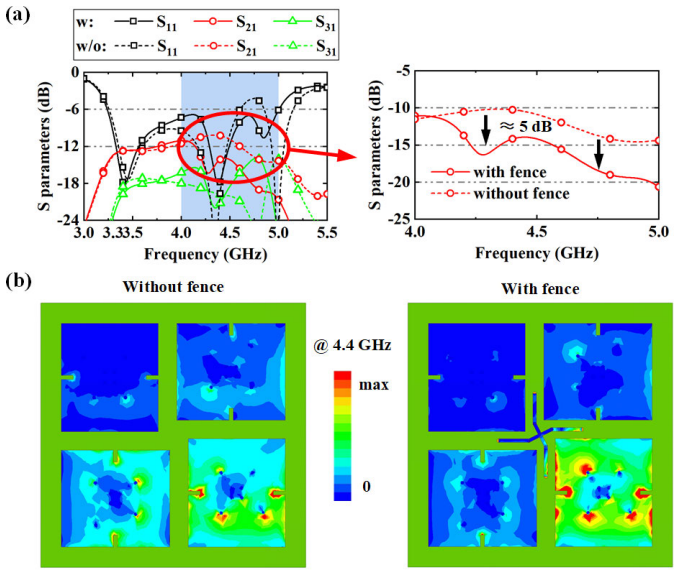

Fig. 9. Comparison of the MIMO antenna with and without the cross-line fence. (a) S-parameters. (b) Surface current distributions on the patches (only Ant 1 is excited).

of common and differential modes cancellation [32], [33] are used to achieve high isolation with simple structures.

In our design, by arranging the adjacent elements vertically, i.e., the long side of Ant 1 is parallel to the wide side of Ant 2, the coupling decreases compared with a parallel arrangement. Furthermore, we add a cross-line fence mainly to improve the isolation of adjacent elements at higher frequencies. It consists of four rotationally symmetric branches, which are placed between two patches. Fig. 9 shows the S-parameters and surface currents in two cases, i.e., with and without the cross-line fence. It can be seen that with identical total dimensions and working frequencies, the isolation (S_{21}) between adjacent elements is improved by 5 dB from 4.1 to 5.0 GHz, while the fence has a limited influence at lower frequencies. Besides, Fig. 9(b) shows a resonant current on the fence and an obvious cancellation of the currents on the adjacent elements. Actually, by adjusting the

TABLE II
PERFORMANCE COMPARISON

Ref.	-6 dB Bandwidth	Profile (λ_L)	Area (λ_L^2)	Area Percentage	Efficiency	Isolation (dB)	Gain (dBi)
[8]	4.4-5.0 GHz	0.012	0.59 × 0.30	100%	42%-86%	> 18	3.1-7.2
[9]	4.4-5.0 GHz	0.018	1.06 × 1.06	48%	40%-50%	> 22	1.9-3.7
[11]	3.3-4.2 GHz	0.026	0.44 × 0.44	13.8%	42%-61%	> 10	N. A.
[13]	3.3-4.2 GHz	0.022	$\pi \times 0.17^2$	6.3%	38%*	> 9.7	N. A.
[14]	3.3-4.2 GHz	0.011	0.46 × 0.46	16.8%	40%-58%	> 9.5	N. A.
[27]	3.3-5.0 GHz	0.110	$\pi \times 0.31^2$	N. A.	84%-90%	> 13	5.2-6.8
Proposed	**3.3-5.0 GHz**	**0.028**	**0.65 × 0.65**	**30.1%**	**55%-82%**	**> 12**	**4.4-8.9**

Area Percentage: antenna area divided by the whole area of the back cover.
*: only average total efficiency in the operating band is given.
λ_L: free-space wavelength at the lowest frequency in the band.

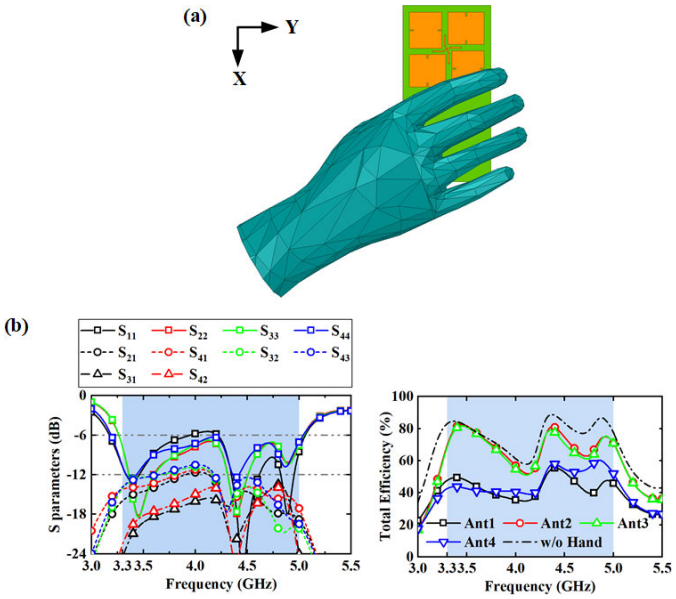

Fig. 10. Analysis of the proposed antenna with a single-hand model. (a) Configuration. (b) S-parameters and total efficiencies.

width of the cross line (w_x), the length of the outer part (x_3), and the whole dimension (l_p), we can obtain a balance between impedance matching and isolation. Finally, isolations over 12 dB are obtained, which fulfills the demand for mobile antennas.

Next, to prove the practicability of the proposed MIMO antenna in real applications, we consider the user's case, where the user holds the mobile phone in one hand. We assume that the MIMO antenna is placed on the top half of the complete back cover of 140 × 70 mm^2. The hand model is provided by HFSS, and the results are given in Fig. 10. The S-parameters are basically the same as the original ones showing similar operating bandwidth and isolations. For the top two elements, the efficiencies are close to the ones in the free-space scenario, which also proves the capability of integration with a full back cover. The other two show a decrease of 20%–40% in efficiency. Nevertheless, the results indicate that the performance of the whole MIMO antenna is robust in real applications.

To better show the novelty of the proposed antenna, Table II gives a comparison between the proposed one and some of the reported literature. It is worth noting that few works have covered all the N77/N78/N79 bands using low-profile planar-type antennas placed on the back cover. Antennas in [8] and [9] achieve a narrower bandwidth with a larger area. Although antennas in [11], [13], and [14] are more compact, they are with a narrower bandwidth and also lower efficiency. The antenna in [27] is proposed for access point applications and has a relatively high profile (10 mm, 0.110 λ_L), which is unable to place on the back cover of the device. Apart from the works in Table II, back cover antennas in [10] and [12] can only cover several narrow bands, whereas Sun et al. [34] and Hei et al. [35] have proposed MIMO antennas with a comparable bandwidth but not based on back cover configurations. In conclusion, compared with previous works, our design shows superiority in bandwidth over previous back cover antennas maintaining a comparable dimension. Besides, it achieves the same bandwidth as the antenna in [27] with a 75% reduction in the profile, thus providing a feasible solution for mobile applications.

V. CONCLUSION

A wideband and low-profile microstrip antenna is proposed for 5G MIMO applications in this communication. By loading two sets of shorting vias and cutting two symmetrical slots on a rectangular patch, triple modes, including the monopole mode, the TM_{10} mode, and the TM_{01} modes, are simultaneously excited to realize wideband radiation. Four antennas are placed in a sequentially rotated configuration with a cross-line fence to improve isolation. The antenna has a total volume of 59.2 × 59.2 × 2.5 mm^3 (0.82 λ_0 × 0.82 λ_0 × 0.034 λ_0). The proposed MIMO antenna covers N77/N78/N79 bands from 3.3 to 5.0 GHz with measured total efficiencies from 55% to 82%. The isolations are over 12 dB and the ECCs are less than 0.05. The proposed four-elements MIMO antenna has the advantages of low profile, compact size, and wideband radiation. It can be placed on the back cover of the device, exhibiting its potential applications in mobile 5G terminals.

ACKNOWLEDGMENT

The authors would like to express our sincere gratitude to Dr. Hanyang Wang from the Consumer Business Group of Huawei Inc., for his kind advice and help in our correspondence.

REFERENCES

[1] Y. Li, Z. Zhang, J. Zheng, and Z. Feng, "Compact heptaband reconfigurable loop antenna for mobile handset," *IEEE Antennas Wireless Propag. Lett.*, vol. 10, pp. 1162–1165, 2011.
[2] Y. Li, Z. Zhang, J. Zheng, Z. Feng, and M. F. Iskander, "A compact hepta-band loop-inverted F reconfigurable antenna for mobile phone," *IEEE Trans. Antennas Propag.*, vol. 60, no. 1, pp. 389–392, Jan. 2012.

[3] J. Choi, W. Hwang, C. You, B. Jung, and W. Hong, "Four-element reconfigurable coupled loop MIMO antenna featuring LTE full-band operation for metallic-rimmed smartphone," *IEEE Trans. Antennas Propag.*, vol. 67, no. 1, pp. 99–107, Jan. 2019.

[4] Z. Xu and C. Deng, "High-isolated MIMO antenna design based on pattern diversity for 5G mobile terminals," *IEEE Antennas Wireless Propag. Lett.*, vol. 19, no. 3, pp. 467–471, Mar. 2020.

[5] C. Deng, D. Liu, and X. Lv, "Tightly arranged four-element MIMO antennas for 5G mobile terminals," *IEEE Trans. Antennas Propag.*, vol. 67, no. 10, pp. 6353–6361, Oct. 2019.

[6] Z. Chen, Y. Liu, T. Yuan, and H. Wong, "A miniaturized MIMO antenna with dual-band for 5G smartphone application," *IEEE Open J. Antennas Propag.*, vol. 4, pp. 111–117, 2023.

[7] W. Hu et al., "Dual-band antenna pair with high isolation using multiple orthogonal modes for 5G smartphones," *IEEE Trans. Antennas Propag.*, vol. 71, no. 2, pp. 1949–1954, Feb. 2023.

[8] B. Cheng and Z. Du, "A wideband low-profile microstrip MIMO antenna for 5G mobile phones," *IEEE Trans. Antennas Propag.*, vol. 70, no. 2, pp. 1476–1481, Feb. 2022.

[9] B. Cheng and Z. Du, "Dual polarization MIMO antenna for 5G mobile phone applications," *IEEE Trans. Antennas Propag.*, vol. 69, no. 7, pp. 4160–4165, Jul. 2021.

[10] L. Chang, G. Zhang, and H. Wang, "Triple-band microstrip patch antenna and its four-antenna module based on half-mode patch for 5G 4×4 MIMO operation," *IEEE Trans. Antennas Propag.*, vol. 70, no. 1, pp. 67–74, Jan. 2022.

[11] K.-L. Wong, M.-F. Jian, and W.-Y. Li, "Low-profile wideband four-corner-fed square patch antenna for 5G MIMO mobile antenna application," *IEEE Antennas Wireless Propag. Lett.*, vol. 20, no. 12, pp. 2554–2558, Dec. 2021.

[12] L. Chang and H. Wang, "Dual-band four-antenna module covering N78/N79 based on PIFA for 5G terminals," *IEEE Antennas Wireless Propag. Lett.*, vol. 21, no. 1, pp. 168–172, Jan. 2022.

[13] L. Chang and H. Wang, "Miniaturized wideband four-antenna module based on dual-mode PIFA for 5G 4×4 MIMO applications," *IEEE Trans. Antennas Propag.*, vol. 69, no. 9, pp. 5297–5304, Sep. 2021.

[14] I. R. R. Barani, K.-L. Wong, Y.-X. Zhang, and W.-Y. Li, "Low-profile wideband conjoined open-slot antennas fed by grounded coplanar waveguides for 4×4 5G MIMO operation," *IEEE Trans. Antennas Propag.*, vol. 68, no. 4, pp. 2646–2657, Apr. 2020.

[15] W. Hu et al., "Wideband back-cover antenna design using dual characteristic modes with high isolation for 5G MIMO smartphone," *IEEE Trans. Antennas Propag.*, vol. 70, no. 7, pp. 5254–5265, Jul. 2022.

[16] Y. Chen, S. Yang, and Z. Nie, "Bandwidth enhancement method for low profile E-shaped microstrip patch antennas," *IEEE Trans. Antennas Propag.*, vol. 58, no. 7, pp. 2442–2447, Jul. 2010.

[17] K.-L. Wong and W.-H. Hsu, "A broad-band rectangular patch antenna with a pair of wide slits," *IEEE Trans. Antennas Propag.*, vol. 49, no. 9, pp. 1345–1347, Sep. 2001.

[18] N.-W. Liu, L. Zhu, W.-W. Choi, and J.-D. Zhang, "A low-profile differentially fed microstrip patch antenna with broad impedance bandwidth under triple-mode resonance," *IEEE Antennas Wireless Propag. Lett.*, vol. 17, no. 8, pp. 1478–1482, Aug. 2018.

[19] N.-W. Liu, L. Zhu, W.-W. Choi, and X. Zhang, "A low-profile aperture-coupled microstrip antenna with enhanced bandwidth under dual resonance," *IEEE Trans. Antennas Propag.*, vol. 65, no. 3, pp. 1055–1062, Mar. 2017.

[20] J. Liu, Q. Xue, H. Wong, H. W. Lai, and Y. Long, "Design and analysis of a low-profile and broadband microstrip monopolar patch antenna," *IEEE Trans. Antennas Propag.*, vol. 61, no. 1, pp. 11–18, Jan. 2013.

[21] Q. Hou, H. Tang, Y. Liu, and X. Zhao, "Dual-frequency and broadband circular patch antennas with a monopole-type pattern based on epsilon-negative transmission line," *IEEE Antennas Wireless Propag. Lett.*, vol. 11, pp. 442–445, 2012.

[22] W. Liu, Z. N. Chen, and X. Qing, "Metamaterial-based low-profile broadband mushroom antenna," *IEEE Trans. Antennas Propag.*, vol. 62, no. 3, pp. 1165–1172, Mar. 2014.

[23] W. Liu, Z. N. Chen, and X. Qing, "Metamaterial-based low-profile broadband aperture-coupled grid-slotted patch antenna," *IEEE Trans. Antennas Propag.*, vol. 63, no. 7, pp. 3325–3329, Jul. 2015.

[24] W. Sun, Y. Li, Z. Zhang, and P.-Y. Chen, "Low-profile and wideband microstrip antenna using quasi-periodic aperture and slot-to-CPW transition," *IEEE Trans. Antennas Propag.*, vol. 67, no. 1, pp. 632–637, Jan. 2019.

[25] W. Sun, Y. Li, Z. Zhang, and Z. Feng, "Broadband and low-profile microstrip antenna using strip-slot hybrid structure," *IEEE Antennas Wireless Propag. Lett.*, vol. 16, pp. 3118–3121, 2017.

[26] Z. Wang, T. Liang, and Y. Dong, "Composite right-/left-handed-based, compact, low-profile, and multifunctional antennas for 5G applications," *IEEE Trans. Antennas Propag.*, vol. 69, no. 10, pp. 6302–6311, Oct. 2021.

[27] K.-L. Wong, J.-Z. Chen, and W.-Y. Li, "Four-port wideband annular-ring patch antenna generating four decoupled waves for 5G multi-input–multi-output access points," *IEEE Trans. Antennas Propag.*, vol. 69, no. 5, pp. 2946–2951, May 2021.

[28] A. Boukarkar, X. Q. Lin, Y. Jiang, L. Y. Nie, P. Mei, and Y. Q. Yu, "A miniaturized extremely close-spaced four-element dual-band MIMO antenna system with polarization and pattern diversity," *IEEE Antennas Wireless Propag. Lett.*, vol. 17, no. 1, pp. 134–137, Jan. 2018.

[29] J. Deng, J. Li, L. Zhao, and L. Guo, "A dual-band inverted-F MIMO antenna with enhanced isolation for WLAN applications," *IEEE Antennas Wireless Propag. Lett.*, vol. 16, pp. 2270–2273, 2017.

[30] S. Shoaib, I. Shoaib, N. Shoaib, X. Chen, and C. G. Parini, "Design and performance study of a dual-element multiband printed monopole antenna array for MIMO terminals," *IEEE Antennas Wireless Propag. Lett.*, vol. 13, pp. 329–332, 2014.

[31] Q. X. Lai, Y. M. Pan, and S. Y. Zheng, "Mode-counteraction based self-decoupling in circularly polarized MIMO microstrip patch array," *IEEE Trans. Antennas Propag.*, vol. 70, no. 10, pp. 9337–9346, Oct. 2022.

[32] L. Sun, Y. Li, Z. Zhang, and H. Wang, "Antenna decoupling by common and differential modes cancellation," *IEEE Trans. Antennas Propag.*, vol. 69, no. 2, pp. 672–682, Feb. 2021.

[33] H. Xu, S. S. Gao, H. Zhou, H. Wang, and Y. Cheng, "A highly integrated MIMO antenna unit: Differential/common mode design," *IEEE Trans. Antennas Propag.*, vol. 67, no. 11, pp. 6724–6734, Nov. 2019.

[34] L. Sun, Y. Li, Z. Zhang, and Z. Feng, "Wideband 5G MIMO antenna with integrated orthogonal-mode dual-antenna pairs for metal-rimmed smartphones," *IEEE Trans. Antennas Propag.*, vol. 68, no. 4, pp. 2494–2503, Apr. 2020.

[35] Y. Q. Hei, J. G. He, and W. T. Li, "Wideband decoupled 8-element MIMO antenna for 5G mobile terminal applications," *IEEE Antennas Wireless Propag. Lett.*, vol. 20, no. 8, pp. 1448–1452, Aug. 2021.